Progress In Electromagnetics Research M, Vol. 52, 119–127, 2016

Analysis and Measurement of Ship Shaft-Rate Magnetic Field in Air

Yu-Hui Sun[1, 2, *], Chun-Sheng Lin[1], Wen-Dou Jia[1], and Guo-Jun Zhai[3]

Abstract—The corrosion and anti-corrosion current of a ship modulated by the shaft can be equivalent to a time-harmonic current. Based on Maxwell's equations and boundary conditions of electromagnetic field, the Helmholtz equation of magnetic vector potential and the magnetic field expressions of the time-harmonic current in air are deduced. Then, the fast Hankel transform filtering algorithm is applied to solve the equations which contain Bessel function integrals. The theoretic calculation indicates that the magnetic induction intensity and its attenuation rate decrease along with the increase of distance. The three components of magnetic field have different distribution. At last, it is verified that the shaft-rate magnetic field can be observed by the experiments of carbon electrodes and ship model carried in a sea pool.

1. INTRODUCTION

In a marine environment, a ship generates several electromagnetic signatures because of structural ferromagnetic, corrosion currents, anti-corrosion currents, and on board equipments [1]. While the ship is sailing, the corrosion and anti-corrosion currents modulated by shaft produce an extremely low frequency (ELF) electromagnetic field with the fundamental frequency equal to the shaft rotation frequency, which is called shaft-rate (SR) electromagnetic field. SR electromagnetic field attenuates very slowly with a fundamental frequency of $1 \sim 7$ Hz, so it can be used as a signal source for remote detection of ships. The SR magnetic field is more susceptible to disturbance by the environment electromagnetic field than electric field. Therefore, it is very difficult to be detected. However, the propagation of the SR magnetic field in air is very close to that in sea, so the SR magnetic field can be applied in aeromagnetic survey. Thus, the detection efficiency can be considerably improved, and its applications can be expanded.

Since the middle of the last century, many researchers have studied ship SR electromagnetic field [2–6]. Owing to high conductivity of the seawater, the actual measurement and equipment mainly concentrated in the SR electric field by using time-harmonic electric dipole model. Lu et al. measured the SR electric field in a sea pool, analyzed the space distribution of the SR electric field, and finally established the model of an ELF time-harmonic horizontal electric dipole in sea [6, 7]. Mao and Lin modeled the electromagnetic fields produced by a moving time-harmonic horizontal electric dipole in two-layer media [8]. Xiong et al. researched the model method of shaft-rate electric filed in shallow sea [9]. Zolotarevskii et al. introduced the development of instruments for measuring such fields [10]. Cheng et al. extracted the line spectrum of the ship shaft-rate electric field based on empirical mode decomposition and fourth-order cumulant [11]. However, the SR magnetic field is so weak that it is rarely researched and reported. Wu et al. calculated and measured the SR magnetic signatures in sea, while the measuring platform was shaking. But the paper did not analyze the magnetic interference of the platform shaking [12]. And Huang et al. derived the magnetic field expression in air produced by time-harmonic current based on an air-sea two-layered model without measurement [13]. With the

Received 16 September 2016, Accepted 17 November 2016, Scheduled 2 December 2016

* Corresponding author: Yu-Hui Sun (sunyh389@163.com).

[1] Department of Weapon Engineering, Naval University of Engineering, Wuhan 430033, China. [2] New Star Research Institute of Applied Technology, Hefei 230031, China. [3] Naval Institute of Hydrographic Surveying and Charting, Tianjin 300061, China.

development of sensor technology for magnetic field, it is possible to detect ships on a far distance by using magnetic sensors.

The goal of the present paper is to analyze the SR magnetic field in air produced by time-harmonic current based on an air-sea-seabed three-layered model and verifies it by experiments of carbon electrodes and ship model in a sea pool.

2. MECHANISM OF THE SR MAGNETIC FIELD

Different metal materials of the hull have different chemical activities, and the electrochemical corrosion can cause the corrosion current. In order to reduce the electrochemical corrosion, the cathodic protection system will produce anti-corrosion current. While the shaft is rotating, the contact resistance between the shaft and the hull is not constant, so the current of the propeller-bearing-hull circuit will be modulated with the shaft rate, and this modulation is called internal modulation. As a result of propeller rotation, the resistance between the propeller and the sea periodically alters. The modulation is called external modulation because of the outside resistance variation. A basic diagram is shown in Fig. 1. According to the basic theories of electromagnetic field, it is known that the time-harmonic current must generate the corresponding time-harmonic magnetic field. In addition, the power frequency current and rotation of the shaft with remanence also generate ELF magnetic field. According to the public document, the current through the shaft modulated by the shaft-hull resistance variation is the main factor of the time-harmonic current, so the SR magnetic field generated by the internal modulation current is the main research subject of this paper.

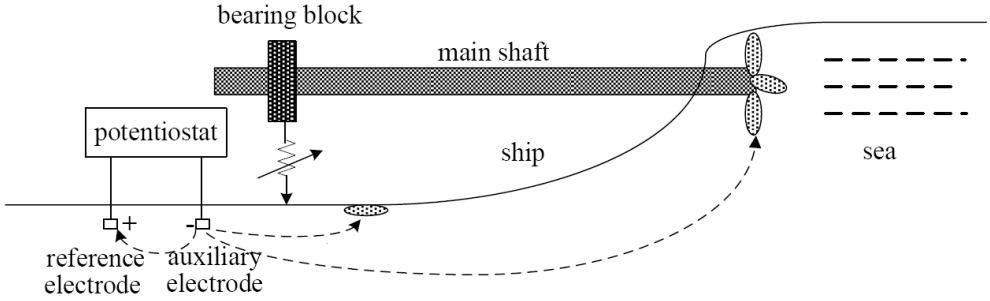

Figure 1. Diagram of ELF signal source modulated by shaft rotating.

3. MODEL OF THE SR MAGNETIC FIELD

As shown in Fig. 2, given that shadow model is an air-sea-seabed horizontal three-layered model, the SR current of a ship is modeled as a horizontal time-harmonic current located in sea layer. In practice, medium 0, medium 1 and medium 2 correspond to air, sea and seabed, respectively. Then the Maxwell equations with time-harmonic form can be described as follows:

$$\begin{cases} \nabla \times \mathbf{H}_i = \mathbf{J}_s + \sigma_i \mathbf{E}_i + \mathrm{j}\omega\varepsilon_i \mathbf{E}_i \\ \nabla \times \mathbf{E}_i = -\mathrm{j}\omega \mathbf{B}_i = -\mathrm{j}\omega\mu_i \mathbf{H}_i \\ \nabla \cdot \mathbf{B}_i = \mu_i \nabla \cdot \mathbf{H}_i = 0 \\ \nabla \cdot \mathbf{D}_i = \rho_e \end{cases} \tag{1}$$

where $\mathbf{H}_i$ is the magnetic field strength, $\mathbf{E}_i$ the electric field strength, $\mathbf{B}_i$ the magnetic induction intensity and $\mathbf{D}_i$ the electric displacement. The three mediums are all uniform, linear and isotropic. σ_i, μ_i, ε_i are conductivity, permeability and permittivity, respectively, and $i = 0, 1, 2$ is medium number.

The expressions of magnetic vector potential $\mathbf{A}$, electric scalar potential ϕ and the Lorenz Gauge can be described as follows:

$$\begin{cases} \mathbf{B} = \nabla \times \mathbf{A} \\ \mathbf{E} = -\nabla\phi - \mathrm{j}\omega \mathbf{A} \\ \nabla \cdot \mathbf{A} - k^2\phi/\mathrm{j}\omega = 0 \end{cases} \tag{2}$$

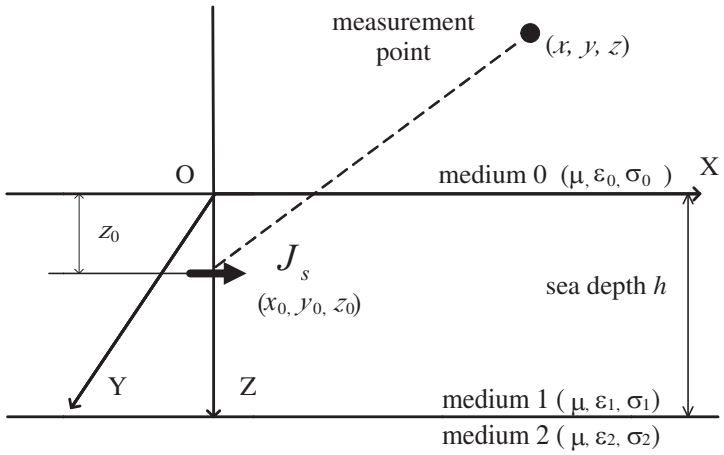

Figure 2. Diagram of the horizontal time-harmonic current in shadow model.

where k is propagation constant, and $k^2 = -\mathrm{j}\omega\mu\sigma + \omega^2\mu\varepsilon$.

According to Eq. (1) and Eq. (2), the Helmholtz equation of magnetic vector potential can be derived as

$$\nabla^2\mathbf{A} + k^2\mathbf{A} = -\mu\mathbf{J}_{\mathrm{S}} \tag{3}$$

The magnetic vector potential $\mathbf{A}_1$ in seawater can be written as $\mathbf{A}_1 = \mathbf{A}_{1p} + \mathbf{A}_{1s}$, where $\mathbf{A}_{1p}$ and $\mathbf{A}_{1s}$ are generated by the primary source and secondary source (the induced current), respectively. $\mathbf{A}_0$ in air and $\mathbf{A}_2$ in seabed can be written as $\mathbf{A}_{0s}$ and $\mathbf{A}_{2s}$, which are generated by the secondary source. The magnetic vector potential generated by the primary source only has X-axis component, and that generated by the secondary source has X-axis and Z-axis component [15].

If the observation distance is $3 \sim 5$ times longer than the horizontal current length, the current can be equal to a horizontal electric dipole. The magnetic vector potential expressions in each medium are assumed, and then the boundary conditions can be utilized to solve the equations. According to the basic formula of Sommerfeld equation, the magnetic vector potential $\mathbf{A}_{1p}$ in medium 1 can be written as

$$\mathbf{A}_{1p} = \frac{\mu_1 Il}{4\pi}\int_0^{+\infty}\frac{\lambda}{\upsilon_1}J_0(\lambda r)e^{-\upsilon_0(z-z_0)}d\lambda\cdot\mathbf{e}_x \tag{4}$$

then the general solution of $\mathbf{A}_0$, $\mathbf{A}_{1s}$ and $\mathbf{A}_2$ can be written as follows [16]:

$$\begin{cases} A_{0x}(\rho,\phi,z) = \sum\limits_{m=-\infty}^{\infty} e^{jm\phi}\int_0^{\infty} J_m(\rho\xi)[a_0(\xi,m)e^{z\upsilon_0} + c_0(\xi,m)e^{-z\upsilon_0}]d\xi \\ A_{0z}(\rho,\phi,z) = \sum\limits_{m=-\infty}^{\infty} e^{jm\phi}\int_0^{\infty} J_m(\rho\xi)[b_0(\xi,m)e^{z\upsilon_0} + d_0(\xi,m)e^{-z\upsilon_0}]d\xi \\ A_{1x}(\rho,\phi,z) = \sum\limits_{m=-\infty}^{\infty} e^{jm\phi}\int_0^{\infty} J_m(\rho\xi)[a_1(\xi,m)e^{z\upsilon_1} + c_1(\xi,m)e^{-z\upsilon_1}]d\xi \\ A_{1z}(\rho,\phi,z) = \sum\limits_{m=-\infty}^{\infty} e^{jm\phi}\int_0^{\infty} J_m(\rho\xi)[b_1(\xi,m)e^{z\upsilon_1} + d_1(\xi,m)e^{-z\upsilon_1}]d\xi \\ A_{2x}(\rho,\phi,z) = \sum\limits_{m=-\infty}^{\infty} e^{jm\phi}\int_0^{\infty} J_m(\rho\xi)[a_2(\xi,m)e^{z\upsilon_2} + c_2(\xi,m)e^{-z\upsilon_2}]d\xi \\ A_{2z}(\rho,\phi,z) = \sum\limits_{m=-\infty}^{\infty} e^{jm\phi}\int_0^{\infty} J_m(\rho\xi)[b_2(\xi,m)e^{z\upsilon_2} + d_2(\xi,m)e^{-z\upsilon_2}]d\xi \end{cases} \tag{5}$$

where $\rho = \sqrt{(x-x_0)^2 + (y-y_0)^2}$,$\phi = \mathrm{arctg}((y-y_0)/(x-x_0))$, $\upsilon = \sqrt{\xi^2 - k^2}$, and $J_m(\rho\xi)$ is the m order Bessel function.

The boundary conditions of electromagnetic field are:

$$\begin{cases} \left[\dfrac{\nabla\cdot\mathbf{A}_{i+1}}{k_{i+1}^2}-\dfrac{\nabla\cdot\mathbf{A}_i}{k_i^2}\right]_{z=d_i}=0 \\ [\mathbf{A}_{(i+1)z}-\mathbf{A}_{iz}]_{z=d_i}=0 \\ [\mathbf{A}_{(i+1)x}-\mathbf{A}_{ix}]_{z=d_i}=0 \\ \left[\dfrac{\partial}{\partial z}\left(\mathbf{A}_{(i+1)x}-\mathbf{A}_{ix}\right)\right]_{z=d_i}=0 \end{cases} \tag{6}$$

When $z\to\pm\infty$, $\mathbf{A}_0$ and $\mathbf{A}_2$ are finite, so there is $c_0(\xi,m)=d_0(\xi,m)=a_2(\xi,m)=b_2(\xi,m)=0$, According to Eq. (6), the m in $a_0(\xi,m)$, $a_1(\xi,m)$, $c_1(\xi,m)$ and $c_2(\xi,m)$ is only equal to 0, and the m in $b_0(\xi,m)$, $b_1(\xi,m)$, $d_1(\xi,m)$ and $d_2(\xi,m)$ is only equal to 1. Then Eq. (5) can be rewritten as

$$\begin{cases} A_{0x}(\rho,\phi,z)=\displaystyle\int_0^\infty J_0(\rho\xi)[a_0(\xi,0)e^{z\upsilon_0}]d\xi \\ A_{0z}(\rho,\phi,z)=\cos\phi\displaystyle\int_0^\infty J_1(\rho\xi)[b_0(\xi,1)e^{z\upsilon_0}]d\xi \\ A_{1z}(\rho,\phi,z)=\displaystyle\int_0^\infty J_0(\rho\xi)[a_1(\xi,0)e^{z\upsilon_1}+c_1(\xi,0)e^{-z\upsilon_1}]d\xi \\ A_{1z}(\rho,\phi,z)=\cos\phi\displaystyle\int_0^\infty J_1(\rho\xi)[b_1(\xi,1)e^{z\upsilon_1}+d_1(\xi,1)e^{-z\upsilon_1}]d\xi \\ A_{2x}(\rho,\phi,z)=\displaystyle\int_0^\infty J_0(\rho\xi)[c_2(\xi,0)e^{-z\upsilon_2}]d\xi \\ A_{2z}(\rho,\phi,z)=\cos\phi\displaystyle\int_0^\infty J_1(\rho\xi)[d_2(\xi,1)e^{-z\upsilon_2}]d\xi \end{cases} \tag{7}$$

According to Eqs. (6) and (7), $\mathbf{A}_0$,$\mathbf{A}_{1s}$, $\mathbf{A}_2$ can be solved. As the object of this paper is $\mathbf{A}_0$ in air, we only write $\mathbf{A}_0$ as follows:

$$\begin{aligned} \mathbf{A}_0 &= \int_0^\infty [\frac{\mu Il}{4\pi}\frac{\xi}{\upsilon_1}e^{-\upsilon_1 z_0}+a_1(\xi,0)+c_1(\xi,0)]e^{z\upsilon_0}J_0(\rho\xi)d\xi\cdot\mathbf{e_x} \\ &\quad +\frac{\partial\rho}{\partial x}\int_0^\infty [b_1(\xi,1)+d_1(\xi,1)]e^{z\upsilon_0}J_1(\rho\xi)d\xi\cdot\mathbf{e_z} \end{aligned} \tag{8}$$

where

$$a_0(\xi,0) = \frac{\mu Il}{4\pi}\frac{\xi}{\upsilon_1}e^{-\upsilon_1 z_0}+a_1(\xi,0)+c_1(\xi,0) \tag{9}$$

$$b_0(\xi,1) = b_1(\xi,1)+d_1(\xi,1) \tag{10}$$

$$c_1(\xi,0) = \frac{\mu Il}{4\pi}\frac{\xi}{\upsilon_1}\frac{(\upsilon_1-\upsilon_2)e^{-\upsilon_1(d-z_0)}+(\upsilon_1+\upsilon_2)e^{\upsilon_1(d-z_0)}}{\dfrac{(\upsilon_0+\upsilon_1)(\upsilon_1+\upsilon_2)}{(\upsilon_1-\upsilon_0)}e^{d\upsilon_1}+(\upsilon_2-\upsilon_1)e^{-d\upsilon_1}} \tag{11}$$

$$a_1(\xi,0) = \frac{(\upsilon_0+\upsilon_1)}{(\upsilon_1-\upsilon_0)}c_1(\xi,0)-\frac{\mu Il}{4\pi}\frac{\xi}{\upsilon_1}e^{-\upsilon_1 z_0} \tag{12}$$

$$\begin{aligned} d_1(\xi,1) &= \upsilon_1(K_1+K_2)e^{d\upsilon_1}a_1(\xi,0)+\upsilon_1(K_1e^{-d\upsilon_1}+K_2e^{d\upsilon_1})c_1(\xi,0) \\ &\quad +\frac{\mu Il}{4\pi}\xi[K_1e^{-\upsilon_1(d-z_0)}+K_2e^{\upsilon_1(d-z_0)}] \end{aligned} \tag{13}$$

$$\begin{aligned} b_1(\xi,1) &= \frac{G_0\upsilon_1+\upsilon_0}{G_0\upsilon_1-\upsilon_0}d_1(\xi,1)+\frac{\xi(G_0-1)}{G_0\upsilon_1-\upsilon_0}[a_1(\xi,0)+c_1(\xi,0)] \\ &\quad +\frac{\mu Il}{4\pi}\frac{\xi^2(G_0-1)}{\upsilon_1(G_0\upsilon_1-\upsilon_0)}e^{-\upsilon_1 z_0} \end{aligned} \tag{14}$$

$$G_0 = k_0^2/k_1^2 \tag{15}$$

$$K_1 = \frac{\xi(1-G_0)(G_0\upsilon_1-\upsilon_0)}{\upsilon_1[(G_0\upsilon_1+\upsilon_0)(G_0\upsilon_2+\upsilon_1)e^{d\upsilon_1}+(G_0\upsilon_1-\upsilon_0)(G_0\upsilon_2-\upsilon_1)e^{-d\upsilon_1}]} \tag{16}$$

$$G_1 = k_1^2/k_2^2 \tag{17}$$

$$K_2 = \frac{\xi(1-G_0)(G_1\upsilon_2+\upsilon_1)}{\upsilon_1[(G_0\upsilon_1+\upsilon_0)(G_1\upsilon_2+\upsilon_1)e^{d\upsilon_1}+(G_0\upsilon_1-\upsilon_0)(G_1\upsilon_2-\upsilon_1)e^{-d\upsilon_1}]} \tag{18}$$

From $\mathbf{B}=\nabla\times\mathbf{A}$ in Eq. (2), the magnetic field expressions can be written as follows:

$$\begin{cases} B_{0x} = \dfrac{\partial^2\rho}{\partial x\partial y}\displaystyle\int_0^\infty b_0(\xi,1)e^{z\upsilon_0}J_1(\rho\xi)d\xi \\ \qquad +\dfrac{\partial\rho}{\partial x}\dfrac{\partial\rho}{\partial y}\displaystyle\int_0^\infty b_0(\xi,1)e^{z\upsilon_0}\xi J_0(\rho\xi)d\xi - \dfrac{\partial\rho}{\partial x}\dfrac{\partial\rho}{\partial y}\dfrac{1}{\rho}\displaystyle\int_0^\infty b_0(\xi,1)e^{z\upsilon_0}J_1(\rho\xi)]d\xi \\ B_{0y} = \displaystyle\int_0^\infty a_0(\xi,0)\upsilon_0 e^{z\upsilon_0}J_0(\rho\xi)d\xi - \dfrac{\partial^2\rho}{\partial x^2}\displaystyle\int_0^\infty b_0(\xi,1)e^{z\upsilon_0}J_1(\rho\xi)d\xi \\ \qquad -\left(\dfrac{\partial\rho}{\partial x}\right)^2\displaystyle\int_0^\infty b_0(\xi,1)e^{z\upsilon_0}\xi J_0(\rho\xi)d\xi + \left(\dfrac{\partial\rho}{\partial x}\right)^2\dfrac{1}{\rho}\displaystyle\int_0^\infty b_0(\xi,1)e^{z\upsilon_0}J_1(\rho\xi)d\xi \\ B_{0z} = -\dfrac{\partial\rho}{\partial y}\displaystyle\int_0^\infty a_0(\xi,0)e^{z\upsilon_0}\xi J_1(\rho\xi)d\xi \end{cases} \tag{19}$$

4. MODEL CALCULATION

In Eq. (19), the Generalized Sommerfeld Integrals contain complex variable factor $e^{\sqrt{\lambda^2-k^2}z}$ and Bessel function $J_n(\lambda r)$, and the numerical computation is complicated. Therefore, this paper adopts the fast Hankel transform which Hu and Nie proposed in 1998 [14].

The frequency of the time-harmonic sine current is 2 Hz, and the strength is $10\,\mathrm{A}\cdot\mathrm{m}$. The electromagnetic parameters of mediums are $\varepsilon_0 = 8.854\times10^{-12}\,\mathrm{F/m}$, $\sigma_0 = 0$, $\varepsilon_1 = 9\varepsilon_0$, $\sigma_1 = 4\,\mathrm{S/m}$, $\varepsilon_2 = 9\varepsilon_0$, $\sigma_2 = 0.04\,\mathrm{S/m}$, and $\mu_0 = \mu_1 = \mu_2 = 4\pi\times10^{-7}\,\mathrm{H/m}$, respectively. The sea depth is 50 m. The source is placed along the X-axis, and the central coordinate is $(0,0,10)$. The measurement point moves along the X-axis, and the start and end are $(-200,50,-10)$ and $(200,50,-10)$. Fig. 3 shows the values of the three components of the magnetic field at each measuring point.

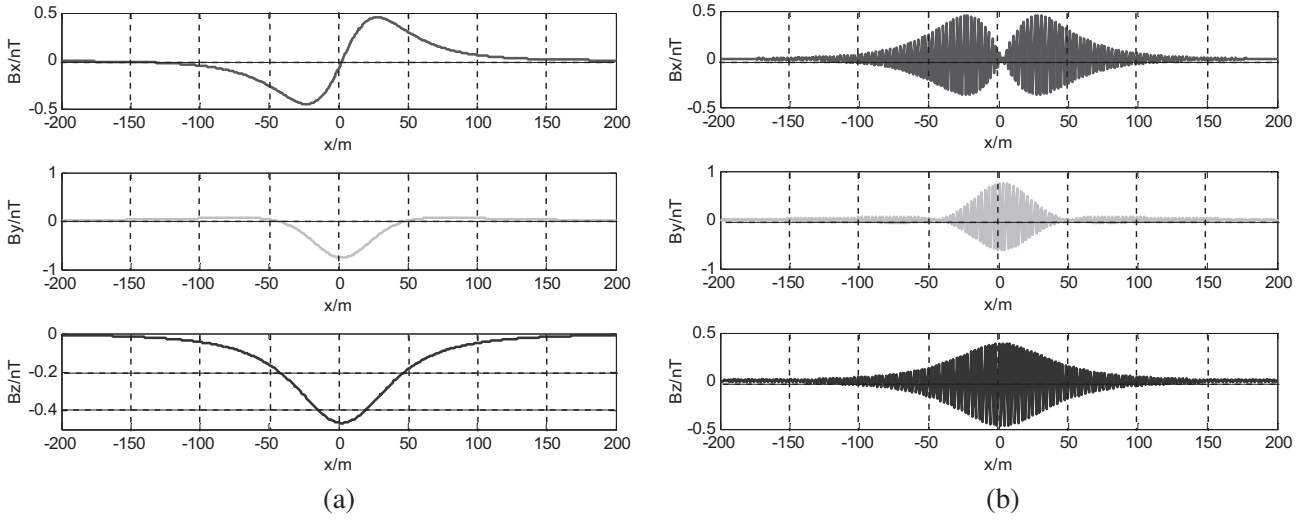

Figure 3. Magnetic field variation law in air. (a) Envelope of the ELF magnetic field. (b) ELF magnetic field.

In Fig. 3, the calculation results accord with the pass-through signatures of ship static electric field [1]. In far field, the magnetic field in air decreases gradually as the distance increases, and the larger the distance is, the more slowly the magnetic field attenuates. Under the above conditions, the maximum of B_x and B_z is smaller than B_y. When the current is $10\,\mathrm{A}\cdot\mathrm{m}$, B_y is more than 0.03 nT at $(150,50,-10)$, and B_x and B_z are about 0.01 nT.

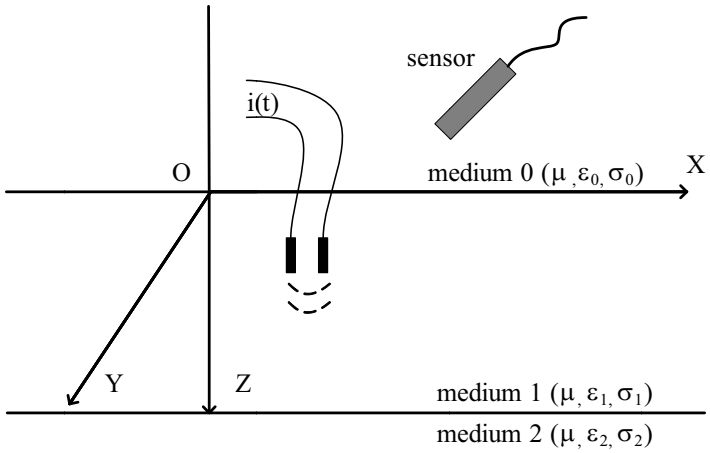

Figure 4. Diagram of electrodes experiment.

5. EXPERIMENTS

The experimental conditions include a non-magnetic pool, two carbon electrodes, a model ship and a magnetic measurement system. The size of the non-magnetic pool is 8 m × 5 m × 1.5 m, and the water depth is 1 m. The water is mixed with industrial salt, and its conductivity is about 4 S/m. The measurement system samples, amplifies and filters the output of the magnetic induction rod, and then it is sent to the host computer through the data acquisition card.

5.1. Carbon Electrodes Experiment

In order to simulate the current, two carbon electrodes are fixed in the water by a bracket, and the ends of the electrodes should be horizontal. The magnetic induction rod and electrodes are shown in Fig. 4.

The rod is placed on the shore and measures the Y-axis component of the magnetic field. The relative position of the sensor and electrodes is $(\Delta x, \Delta y, \Delta z) = (0, 1.7, 1.2)$. Different sinusoidal currents in the circuit are loaded, and the measurements are shown in Fig. 5.

Figure 5(a) represents the ambient magnetic noise and shows that the power spectrum is very even. Figs. 5(b)–(d) represent the time and frequency domain features of the magnetic field when the current is 20 mA, 50 mA and 70 mA. Especially in Figs. 5(c)–(d), the magnetic field is periodic in the time domain and has an obvious line spectrum in the frequency domain. One can conclude that the ELF magnetic field in air can be detected and recognized.

5.2. Ship Model Experiment

The ship model is a scaled-down version of a real ship, and the length is about 2 m. The model hull is composed of steel plates, and in order to increase the corrosion current, the zinc skin is packaged on the hull. As shown in Fig. 6, the ship model is fixed on an aluminous frame, and the propeller and the lower part are immersed in water. It should also be guaranteed that the ship model is still, and the propeller rotates.

The magnetic induction rod is placed on the shore, and the Y-axis component of the magnetic field in air is still measured. The relative position of the rod and the ship model is $(\Delta x,\ \Delta y,\ \Delta z) = (0, 3, 1.2)$. Fig. 7 shows the SR magnetic field when the propeller rotates.

In this experiment, the sea pool and lab are so small that we only measure the magnetic field in a short range. From the time domain waveform, there is more interference than the signal of electrodes. However, the frequency domain feature is quite obvious, and the line spectrum can be recognized easily. It should be explained that the ship model has two propellers, so in the frequency domain chart there are two fundamental frequencies, 2.5 Hz and 2.72 Hz, and the second and third harmonics are also in pairs. Because the sample frequency is 20 Hz, high harmonics are ignored.

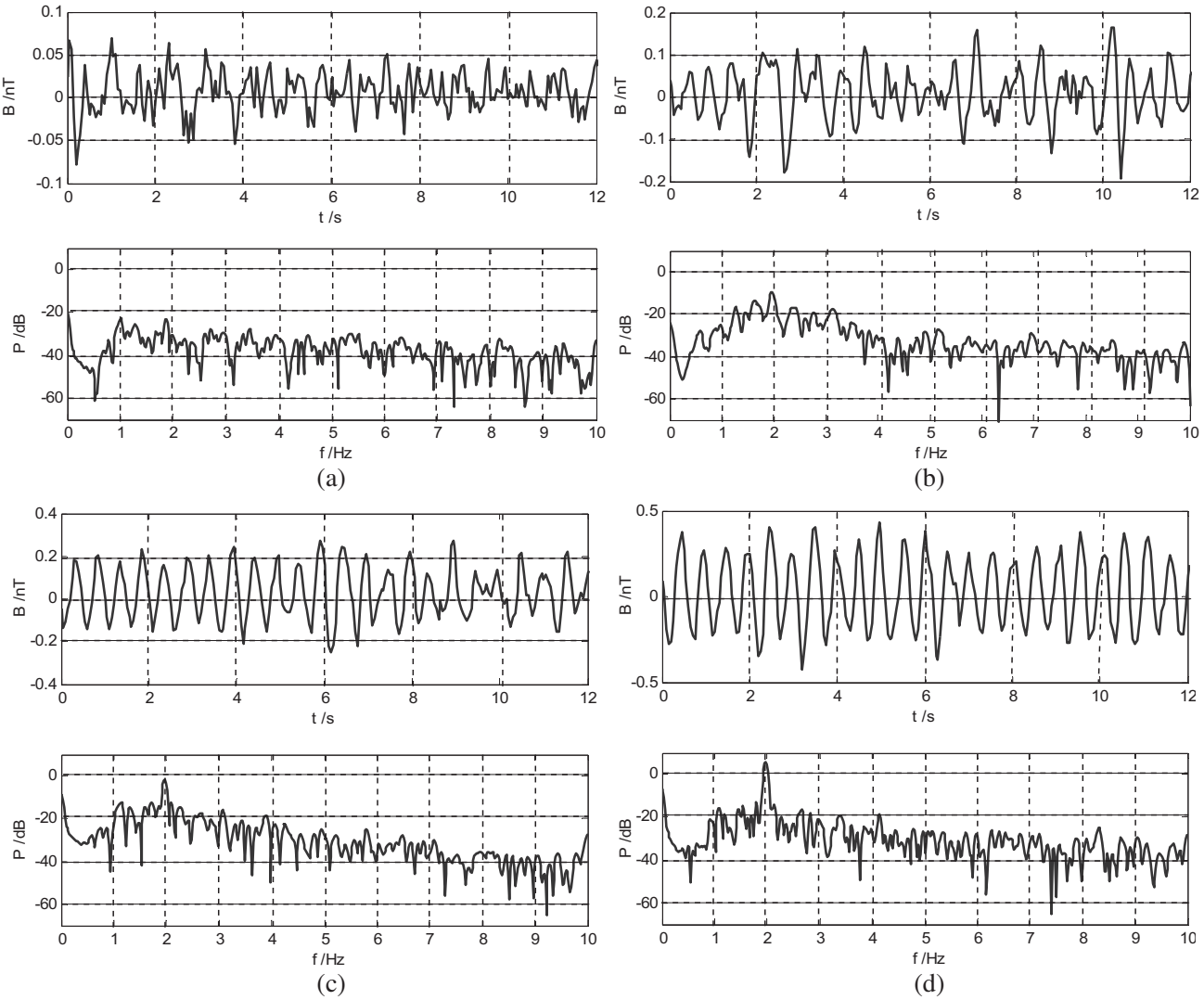

Figure 5. ELF magnetic field generated by the carbon electrodes. (a) Ambient magnetic noise. (b) Peak current is 20 mA. (c) Peak current is 50 mA. (d) Peak current is 70 mA.

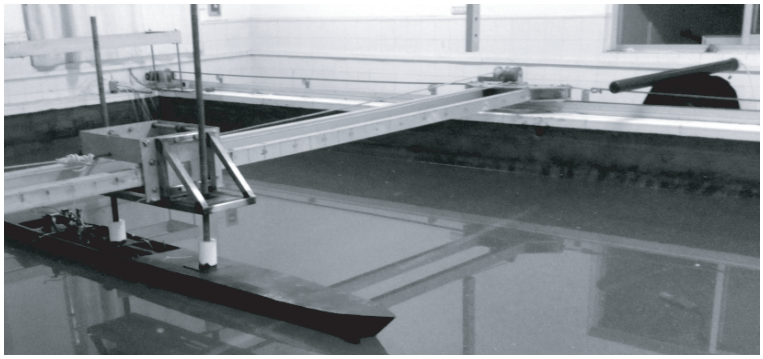

Figure 6. Ship model experiment.

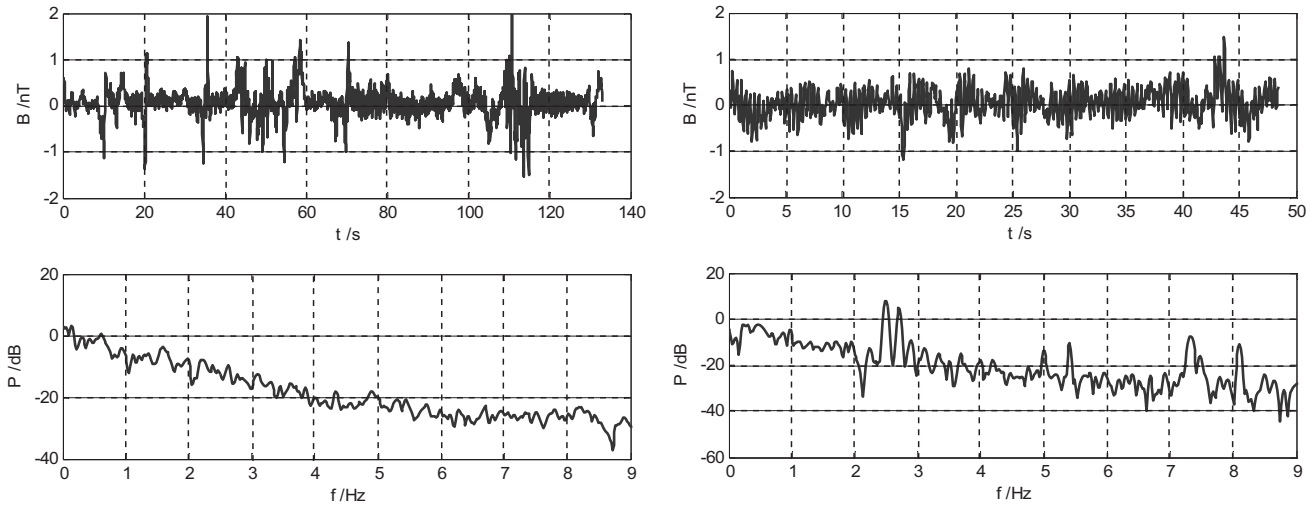

Figure 7. SR magnetic field generated by the ship model.

Compared with the carbon electrodes experiment, the value and signal-to-noise ratio of the ELF magnetic field in air generated by a ship model are smaller. Therefore, it will be hard to detect the signal with the increase of the detection range and the environmental noise sources.

6. CONCLUSIONS

In this paper, detailed analytical expressions have been derived for the ELF magnetic field generated by a time-harmonic horizontal current based on an air-sea-seabed three-layered model. The numerical calculations of the magnetic field, when the source is located in sea and the observation point located in air, are performed and illustrated. And the carbon electrodes experiment and ship model experiment are carried out in a sea pool.

The main conclusions obtained in present paper are summarized as follows.

(1) The corrosion and anti-corrosion current modulated by the shaft can be equivalent to a time-harmonic current. Nowadays, many magnetic sensors have higher resolution than 0.01 nT, even 1 pT, so the SR magnetic field in air can be measured at large distances.

(2) In this paper, the Y-axis and Z-axis components of the magnetic field are higher than X-axis component while $x = 0$. But when the sensor is at other observation points, the above relationship may not be right. In the frequency domain, the line spectrum of the SR magnetic field is so obvious that it can be employed in detecting. If the ambient noises can be eliminated or reduced well, remote detection of ships by using SR magnetic field can be realized.

Though the SR magnetic field of ship can be a signal source of aerial survey to realize remote and rapid detection, and make extremely important military significance, the following questions should be noted:

(1) In the marine environment, the magnetic noise is so complicated that the signal-to-noise ratio of the SR magnetic field is very low. Therefore, better filter techniques are needed to suppress environmental noise in order to improve the signal-to-noise ratio of magnetic field.

(2) For our own ships, how to reduce or even eliminate the SR magnetic field signal to avoid being detected should be further studied.

ACKNOWLEDGMENT

This paper is sponsored by the National Natural Science Foundation of China (No. 41374018, 41476087) and National Major Scientific Research Equipment Development Fund Project (No. ZDYZ2012-1).

REFERENCES

1. Lin, C. S. and S. G. Gong, *Ship Physical Field*, Weapon Industry Press, Beijing, 2007.
2. Hoitham, P., I. Jeffery, B. Brooking, and T. Richard, "Electromagnetic signature modeling and reduction," *Conference Proceeding UDT Europe*, 1999.
3. Bostick, F., H. Smith, and J. Boehl, "The detection of ULF-ELF emissions from moving ships," State Academic Educational Institutions, New York, 1977
4. Timonov, A., I. Barrolade, and P. Holtham, "Generalized ELF propagation," *Proc. Marelec 1997*, 1997.
5. Wait, J. R., "Propagation of radio waves over a stratified ground," *Geophysics*, Vol. 18, No. 2, 1953.
6. Lu, X. C., S. G. Gong, and M. Sun, "Measurement of extremely low frequency field caused by shaft-rate modulated corrosion current," *Acta Armamentarii*, Vol. 25, No. 5, 544–546, 2004.
7. Lu, X. C., S. G. Gong, and M. Sun, "Measurement and analysis of space distribution of shaft-rate electric field of a ship," *Journal of Wuhan University of Technology (Transportation Science & Engineering)*, Vol. 28, No. 4, 498–500, 2004.
8. Mao, W. and C. S. Lin, "The EM fields produced by a moving horizontally-directed time-harmonic dipole in two-layer media," *Acta Armamentarii*, Vol. 30, No. 5, 550–560, 2009.
9. Xiong, L., R. X. Jiang, and S. G. Gong, "Ship modeling method of shaft-ELFE in shallow sea," *Journal of National University of Defense Technology*, Vol. 36, No. 1, 98–103, 2013.
10. Zolotarevskii, Y., F. Bulygin, and A. Ponomarev, "Methods of measuring the low-frequency electric and magnetic fields of ships," *Measurement Techniques*, Vol. 48, No. 11, 1140–1144, 2005
11. Cheng, R., R. X. Jiang, and S. G. Gong, "Extraction of line spectrum of the ship shaft-rate electric field based on EMD and fourth-order cumulant," *Ship Science and Technology*, Vol. 38, No. 1, 94–98, 2016.
12. Wu, Z. Q., X. H. Zhu, and B. Li, "Modeling and measurements of alternating magnetic signatures of ships," *Sensor & Transducers*, Vol. 186, No. 3, 161–167, 2015
13. Huang, F., C. S. Lin, and Z. Y. Yang, "Calculation of electric field produced by a horizontal dipole immersed in shallow sea with anisotropic seabed medium," *Journal of Naval University of Engineering*, Vol. 23, No. 6, 81–85, 2011.
14. Hu, P. and Z. P. Nie, "A new method to calculate Sommerfeld integral-fast hankel transform," *Acta Electronica Sinica*, Vol. 26, No. 3, 126–128, 1998.
15. Lei, Y. Z., *Analytic Method of Time-harmonic Electromagnetic Field*, Science Press, Beijing, 2000.
16. Zhang, Q. G., *Field Theory*, Geological Publishing House, Beijing, 1988.